Chapter 7

Individual Facial Expressions

Besides the static soft tissue prediction, the estimation of postoperative facial emotion expressions is another important criterion for the evaluation of the craniofacial surgery planning. The human face is an important and complex object of human perception. Thus, the patients with facial deformities or paralysis are severely limited in their abilities to the facial emotion expression and cannot convey the normal social signals of interpersonal communication. In such cases, the reestablishment of the aesthetical appearance and normal facial expressions is the primary concern of the corrective surgical impact.

First, we summarize the particular goal of the estimation of facial emotion expressions within the scope of the craniofacial surgery planning more precisely. Of course, the whole spectrum of individual facial emotion expressions is much more complex as it can ever be covered on the basis of abstract mechanical models only. Because of a lack of information on the timing of individual muscular contractions in our approach, the facial animation sequences, which we are able to produce, will generally remain subjective. Nevertheless, consistent biomechanical modeling of facial expressions on the basis of individual anatomical models derived from tomographic data should yield some important insights about physically possible individual facial emotion expressions. In fact, we are not pretending to predict a typical smile of those individual, but one of his/her *physically possible* expression of happiness. This can be also formulated as follows: for example, the facial expressions we are going to estimate are not necessarily the *typical* individual facial emotion expressions, but he/she should in turn be able to mime the way we figured. Besides the modeling of complex facial emotion expressions, the estimation of single muscle actions is of great interest for the non-surgical facial nerve rehabilitation [63].

The content of this chapter is as follows. After the review of the existing lit-

erature related to the topic of facial animation and muscle modeling, we describe our approach for the modeling of contracting muscles and the estimation of individual facial expressions. Finally, the experimental results of facial expression simulations are presented.

7.1 Facial Animation

The complexity of the human face makes it a challenging subject for modelers. It benefits from and can contribute to the larger field of human body modeling. Facial modeling is a multidisciplinary effort, which has links to many other fields such as medicine and engineering. In the last three decades, many research groups have made their substantial contributions to this complex and fascinating field of study. In view of particular goals, different techniques have been developed. Generally, the collective term of facial animation comprehends following three disciplines [96]

- facial expression,
- facial conformation,
- lip motion (for speech synchronization).

The goal of the facial expression modeling is the modeling of the six canonical expressions of happiness, anger, fear, surprise, disgust and sadness. Conformation control specifies individual faces from the universe of possible face prototypes that can be also associated with morphological or long-term facial changes, such as growth or aging. Lip synchronization concerns the coordination of the jaw, lip, and mouth parts with real or synthetic speech samples. In this work, we focus on the estimation of basic facial expressions only.

Four distinctive control techniques are known in the facial animation. These are

1. 3D shape interpolation,
2. ad hoc surface shape parameterization,
3. muscle-based, or abstract muscle models and
4. physically based models.

Each technique possesses particular advantages and disadvantages.

Shape interpolation is an early simple technique to control synthetic faces [91]. It operates on a database of discrete facial postures, which are created from 3D digitizers or optical scanners. These facial datasets have the property of topological equivalence such that a complete mapping can be found for each vertex in every facial posture. Once a complete set is derived, then in between interpolation of the coordinates can be computed. Unfortunately, this technique is limited to the set of predefined facial postures, which prompted the development of parameterization schemes.

The objective of facial parameterization is to describe the face with a small set of control parameters [92, 93]. These parameters are hard-wired into a particular facial geometry and the parameters are only loosely based on the dynamics of the facial expression. For example, the expression on the brow from surprise involves the manipulation of five or six vertices of the facial geometry. Alternatively, distances measured between some facial landmarks (such as lip internal height or width) can be used to predict 3D parametric contour functions. This is particularly useful in the case of the lips, which follow regular rules of deformation. Landmark-based techniques are very popular in computer graphics, since they are efficient and flexible, when animating some cartoon-based characters. An example of this approach is the *motion-capturing technique* [39], which is based on the monitoring of the facial landmarks movements in the source image and their mapping onto the target image. The main advantage of this approach is the adoption of the natural timing of human facial emotion expressions. Animated animals and human characters in the recent computer animation based movies are realized with the help of this technique. Obviously, the motion capturing is not suited for the estimation of individual facial expressions.

Muscle-based models or abstract-muscle models mimic at a simple level the action of three primary muscle groups of the face: (1) the linear, such as the zygomaticus major, (2) the sphincter, such as the orbicularis oculi, and (3) the sheet such as the frontalis major [94, 82, 116]. This approach has also been extended to B-spline surfaces [115]. There are two distinct advantages for these models: they are independent of particular facial geometry and they map directly into muscle-based coding systems.

Physically based models attempt to model the shape and dynamic changes of the face by modeling the underlying properties of facial tissue and muscle action [113, 100, 101]. Most of these models are based on mass-spring or FE meshes with muscle actions approximated by a variety of force functions. These models are computationally expensive and difficult to control with force-based functions. As an example of this approach, in [71, 72] a framework for the estimation of

facial expressions based on a linear elastic FE model of soft tissue and a heuristic parametrization of the mimic muscles is presented.

Typically, the validity of facial animation sequences is done by visual inspection. For example, does it look right? Such criterion might be sufficient for semi-realistic, cartoon-based faces. However, the goal of the facial expression simulation within the scope of craniofacial surgery planning is to estimate the *individual* facial expressions. Simplified approaches, which do not consider individual anatomy and correct tissue biomechanics, are not adequate for that purpose. From this point of view, there seems to be no alternative to consistent physical modeling of contracting muscles and muscle-tissue interaction on the basis of underlying biomechanical laws.

7.2 Anatomy and Physiology of Muscles

The main macroscopic property of muscle is its ability to contract. In accordance with the sliding filament theory, this macroscopic property is effected through the shortening of muscle fibers that consist of two main contractile proteins (*actin*, *myosin*) and several other protein structures building a separate morphological unit, the so-called *sarcomer* [44]. Thereby, muscle fibers do get shorter due to a sort of sliding of the myofilaments across each other. The shortening of the serially arranged sarcomers develop a tension along their longitudinal axis. Sarcomers represent the lowest level of the complex hierarchical structure of muscles, which is shown in Figure 7.1. The muscle fibers group themselves into bundles known as fascicles, which are in turn enveloped by a material known as fascia. Each fascia group represents different heads of a muscle. Within the fascia, the muscle fibers can have an orientation characterized by the angle they make with respect to the tendons they attach to. This fiber arrangement is known as the muscle pennation. Figure 7.2 illustrates several types of pennation patterns of skeletal muscle. The pennation patterns of facial muscles can be reduced to three main types already mentioned above: linear, sphincter and sheet.

The arrangements of muscle fibers determine the direction of the produced forces. Muscles can attach to tendon material either at a narrow site or over wide sheets of tendon known as aponeurosis. As both muscle and tendon work closely together to create a functional unit of force generation and transmission, they are often referred as a collective biomechanical structure, a *musculotendon unit*.

Tendon is made up of parallel-aligned collagen fibers (cf. Figure 3.1), which are several orders of magnitude stiffer than muscle, cf. Table 5.1. Therefore, the

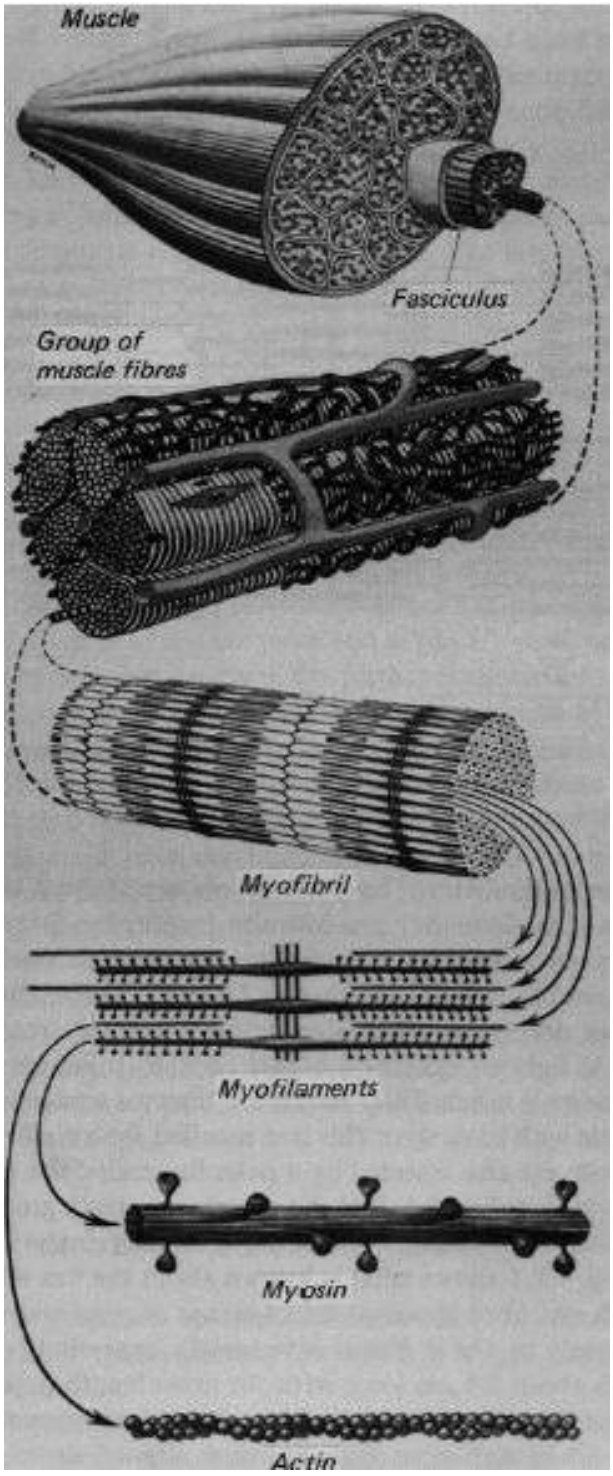

Figure 7.1: Hierarchical structure of muscles (from [44]).

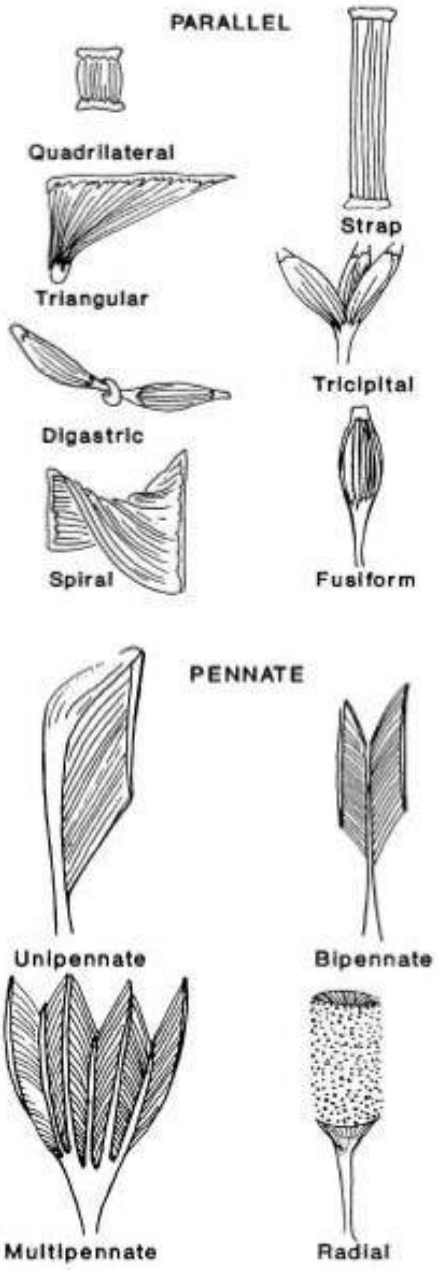

Figure 7.2: Pennation patterns of skeletal muscles (from [85]).

areas where tendon is in contact with muscle have restricted movement compared to the uncovered portions of muscle. The tendon portion of the skeletal musculotendon unit attached to bone at two different sites known as the origin and the insertion. Facial muscles differ from most other skeletal muscles in several significant ways. In particular, some mimic muscles are attached to soft tissue or other muscles. In this case, we call the tendon portion of the musculotendon unit attaches to bone the origin and those connected to soft tissue the insertion.

7.3 Biomechanical Models of Contracting Muscles

Any consistent geometrical and physical model of the musculotendon unit should capture the aspects of muscle anatomy and physiology described above. Putting it all together, muscles are represented in the geometrical model by their shape and in the biomechanical model of deformable soft tissue by the forces acting along the fiber tangents. Being vectorial variable, the force is characterized by the magnitude and the direction. For an arbitrary shaped muscle occupying the domain Ω_{muscle}, both the magnitude and the direction of the spatially distributed force density $\mathbf{f}(\mathbf{x})$ are unknown functions of coordinates. For dynamical simulations of muscle contraction, time dependence of natural muscle activation patterns $\mathbf{f}(\mathbf{x}, t)$ is additionally to be taken into account.

Hence, we firstly review existing abstract muscle models. The majority of these works has been done on the field of musculoskeletal biomechanics. However, some general principles are still valid for any contracting muscles, including the facial musculature.

One of the earliest models of contracting muscle extensively used in later works is the so-called Hill's model [58]. It is based on a series of controlled experiments on muscle, namely the force-length and force-velocity dependencies observed in active muscle. The model has three major components: the series element (SE), the parallel element (PE) and the contractile element (CE). In the simplified models, one of these elements can be removed, if they do not have a significant effect on forces generated. The series element (SE) describes the effects of several biological materials in musculotendon. This element represents mainly the elastic effects of tendon and intrinsic elasticity of structures within the sarcomer. The parallel element (PE) represents passive elastic properties of the connective tissue sheaths (fascia) of the muscle. Due to the material properties of these sheaths, tension is only produced when the PE is actively strained beyond its rest length. The contractile element (CE) contains the source of active force generation. The total muscle response in Hill's models is described by the force-

length function $f(l_m)$, which contains several modeling constants to be fitted to the experimental results. Most further investigations on muscle contraction modeling have been focused on the force-length-velocity relationship.

In [120], an improvement of the Hill's model is proposed that includes the complete modeling of the contraction dynamics $f(l_m, t)$ considering the musculotendon architecture, the force-length and force-velocity relations, and the activation dynamics. The muscle actuator in their approach is modeled as composed of a linear spring for tendon, in pennation with a Hill type model of muscle.

Hill's models provide the magnitude of the muscle forces. However, they do not consider the muscle geometry determines the direction of the force vectors or *lines of action*. For arbitrary shaped muscle, lines of action have to be interpolated with the help of any suitable modeling technique that considers the unique arrangements of muscle fibers.

A finite element model of skeletal muscle for computer animation, including the interpolation of lines of action, is proposed in [18]. The FE analysis is firstly performed on a prismatic, generic model. The resulting deformations were then mapped onto the particular muscle using the free-form deformation technique. In their approach, muscle is considered as a homogeneous, incompressible, isotropic, linear viscoelastic material being under the impact of the time-dependent force density $\mathbf{F}(t)$, cf.(2.2)

$$M\frac{\partial^2 \mathbf{u}}{\partial t^2} + C\frac{\partial \mathbf{u}}{\partial t} + K\mathbf{u} = \mathbf{F}(t)\,, \tag{7.1}$$

where $\mathbf{u}$ is the nodal displacement. M, C and K are the mass, dumping and stiffness matrices, respectively. Similar approach for biomechanical simulation of contracting muscles on the basis of CT/MRI volume data can be found in [122].

In [98], Peskin et al. constructed their *Immersed Elastic Fibers* for modeling the heart muscle. The constitutive equation of the composite material consisting of fluid and fibers is given by

$$\sigma_{ij} = -p\delta_{ij} + 2\mu e_{ij} + T\tau_i\tau_j\,, \tag{7.2}$$

where σ_{ij} is the stress tensor, p is the fluid pressure, μ is the constant of the fluid viscosity, $e_{ij} = 0.5(\partial_j u_i + \partial_i u_j)$ is the linearized strain tensor, T is the fiber tension (force per unit cross-sectional area of composite) and τ_i is the unit fiber tangent. The associated boundary value problem is discretized by using the finite difference method. Based on this approach, the vibrations of an artificial model,

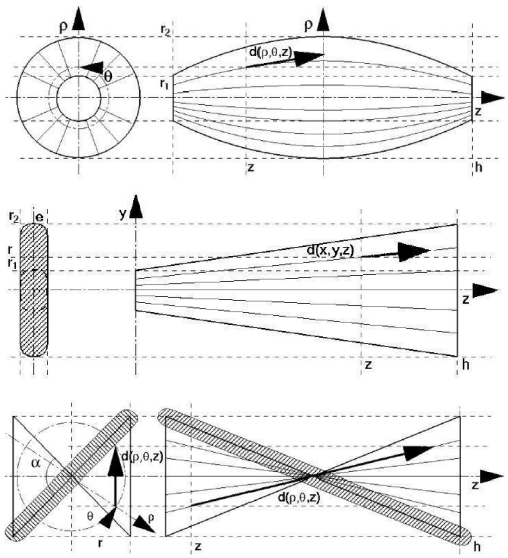

Figure 7.3: Fusiform, triangular and spiral muscle description (from [85]).

an immersed fiber-wound toroidal tube with two predefined layers of fibers is simulated.

The major difficulty of the *macroscopical modeling* of muscles is the lack of information on the unique, spatial arrangement of *microstructures*, e.g., muscle fibers determining lines of acting forces. Especially in muscle-based facial animation, an adequate interpolation of muscle forces is important for the realism of the resulting facial expression simulation. In previous works, a variety of heuristic constructions considering the muscle anatomy has been proposed. Most of these models use the mainline of muscle, i.e., the line connecting the origin and insertion areas, as line of action. Such mainline related model is used for the modeling of muscle-based facial expressions in [71, 72]. A model based on the fusiform interpolation of skeletal muscles is proposed in [106]. An interesting approach for the interpolation of skeletal muscle forces based on B-spline technique is proposed in [89]. In [85], it has been intuitively remarked that muscle fibers are organized resembling a flow, similar to the flow-lines considered in fluid mechanics or in electromagnetism. Muscles may be viewed as continuous fibrous objects, which may be described by the means of a vector field acting along the fiber tangents. However, the author further considers only three predefined types of the pennation patterns: fusiform, triangular and spiral, see Figure 7.3. Any arbitrary shaped muscle can then be represented by means of scaling of these three generic muscle types.

7.4 Virtual Fibers

Since none of the existing approaches known from the literature provides an ultimate solution for the biomechanical modeling of facial musculature, an alternative approach for modeling of individual muscle-based facial expressions is developed in this work.

In our approach, individual anatomy is represented in the geometrical model by the triangulated surfaces, which correspond to the boundaries between essential anatomical structures. However, the information on microscopic structures such as fibers in muscles and skin needed for biomechanical modeling of anisotropic behavior of these tissues is completely missing. In geometrical models, muscles are represented by the shapes of their infolding capsules. Since the information on microscopic structures such as muscle fibers cannot be obtained from tomographic data, any suitable construction considering the natural relationship between muscle shape and its biomechanical functionality can be applied for the interpolation of spatial fiber arrangements.

Our approach for the estimation of individual facial expressions is based on the shape-based, heuristic construction of *Virtual Fibers* [52], which enables the interpolation of muscle forces for an arbitrary shaped muscle embedded in the general FE model of deformable facial tissue. In what follows, the essential statements of this approach are described.

Muscle forces. In the general FE model of deformable soft tissue, each muscle is represented by the $3 \times N$ vector of nodal loads $\mathbf{f}$, where N is the number of mesh nodes, acting inside of the subdomain $\Omega_{\text{muscle}} \subset \Omega$ along the direction of fiber tangents $\boldsymbol{\tau} : |\boldsymbol{\tau}| = 1$

$$\mathbf{f}(\mathbf{x}) = \begin{cases} \lambda(\mathbf{x})\,\boldsymbol{\tau}(\mathbf{x}) & \mathbf{x} \in \Omega_{\text{muscle}} \subset \Omega \\ 0 & \text{else} \end{cases} \tag{7.3}$$

where λ is the magnitude of the force density. Both $\lambda(\mathbf{x})$ and $\boldsymbol{\tau}(\mathbf{x})$ are generally unknown functions of coordinates $\mathbf{x}$.

Lines of action. The exact orientation of muscle fibers, i.e., the vector field of fiber tangents $\boldsymbol{\tau}(\mathbf{x})$ in (7.3), which determines lines of acting forces, is unknown. The following construction is applied to interpolate $\boldsymbol{\tau}(\mathbf{x})$ for the given muscle shape $\Gamma_{\text{muscle}} \subset \Omega_{\text{muscle}}$. Macroscopically seen, muscle fibers enveloped by the muscle capsule Γ_3 connect two or more origin and insertion areas $\Gamma_{1,2}$, see Figure 7.4. The family of such geodesic curves reflecting the shape of the mus-

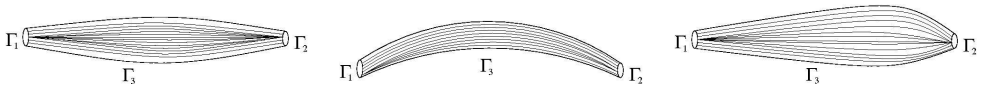

Figure 7.4: Schematic model of muscle: orientation of fibers connecting the origin and insertion areas of muscle $\Gamma_{1,2}$ reflects the muscle shape Γ_3.

cle capsule seems in fact to yield a feasible interpolation of the natural fiber arrangement and resembles the iso-lines of a vector field observed in computational thermodynamics, electromagnetismus, fluid or continuum mechanics. Accordingly, the spatial arrangement of muscle fibers can be obtained as a solution of the boundary value problem given by the partial differential equation of mathematical physics (PDEMF) and suitably defined boundary conditions. There is no particular reason, which would make the interpolation technique based on one PDEMF more accurate or advantageous in comparison with the others. However, we can imagine that at least one remark probably makes sense: the resulting vector field $\boldsymbol{\tau}(\mathbf{x})$ should be preferably curl-free

$$[\boldsymbol{\nabla} \times \boldsymbol{\tau}] = 0\,, \tag{7.4}$$

which considers the fact that muscle fibers do not form knots. From (7.4), it follows that $\boldsymbol{\tau}$ is a gradient field

$$\boldsymbol{\tau}(\mathbf{x}) = \boldsymbol{\nabla}\psi(\mathbf{x})\,, \tag{7.5}$$

where $\psi(\mathbf{x})$ is some scalar function of coordinates. Thus, the solution of the Laplace PDE

$$\boldsymbol{\nabla}\boldsymbol{\tau}(\mathbf{x}) = \boldsymbol{\Delta}\psi(\mathbf{x}) = 0 \quad \mathbf{x} \in \Omega_{\text{muscle}} \subset \Omega \tag{7.6}$$

with appropriate boundary conditions on $\Gamma_{\text{muscle}} \subset \Omega_{\text{muscle}}$ will yield the curl-free vector field in the subdomainΩ_{muscle} occupied by muscle.

However, in this work, we decided uniformly to use the PDEMF-solver already available with our general FE platform based on continuum mechanics. In this approach, we obtain the interpolating field of fiber tangents as a kind of*test deformation* of the subdomain Ω_{muscle} corresponding to the muscle. Consider the schematic model of an unilateral muscle, cf. Figure 7.4. The test deformation yielding the vector field of*virtual fiber tangents* is given by the following linear

elastic BVP

$$\begin{cases} (1-2\nu)\boldsymbol{\Delta\tau} + \text{grad}\,\text{div}\,\boldsymbol{\tau} = 0 \\ \boldsymbol{\tau}(\mathbf{x}) = \begin{cases} -\mathbf{n} & \mathbf{x} \in \Gamma_1 \subset \Omega_{\text{muscle}} \\ \mathbf{n} & \mathbf{x} \in \Gamma_2 \subset \Omega_{\text{muscle}} \\ 0 & \mathbf{x} \in \Gamma_3 \subset \Omega_{\text{muscle}} \end{cases} \end{cases} \tag{7.7}$$

where $\mathbf{n}$ is the outer surface normal. The solution of (7.7) yields a kind of fbw-fi eld running inside of Ω_{muscle} from the insertion Γ_1 (e.g., contact surface to soft tissue) to the origin Γ_2 (e.g., contact surface to bone), see Figure 7.5. The areas $\Gamma_i \subset \Gamma_{\text{muscle}}$ are essential for the computation of an adequate fbw-fi eld and have to be assigned according to the particular muscle shape and its natural anatomic connectivity. This process is usually done during the segmentation stage. Subsequently, the vectors $\boldsymbol{\tau}$ obtained as a solution of (7.7) are to be normalized. The Poisson ratio ν in (7.7) can be used for a slight control on the vector orientation.

Force magnitude. In the fi rst approximation, the magnitude of the muscle forces acting along the lines of action $\boldsymbol{\tau}$ may be assumed coordinate-independent $\lambda \in [0, \lambda_{\text{max}}]$ in the whole domain occupied by a muscle. The value λ_{max} corresponding to the maximum allowed contraction for the particular muscle has to be determined empirically by adapting to experimental results.

Insertion area. Muscle fi bers do not abruptly end in the insertion area. In fact, they branch out to surrounding soft tissue or other muscles. The spatial arrangement of muscle fi bers in the insertion area decisively determines the main zone of muscle action and is essential for the correct modeling of resulting muscle forces. In our approach, we model the insertion area as a cone-shaped prolongation of muscle subdomain Ω_{muscle} characterized by the effective radius of action R and the apex angle α, see Figure 7.6. The magnitude of the muscle forces acting within the insertion area differs from those inside of muscle and has also to be determined empirically.

7.5 Experimental Results

In this section, the experimental results related to facial expression simulations are presented. We start with the validation of the Virtual Fibers approach with artifi cial muscle models. Then, we present the simulations of the individual, muscle-based facial expressions.

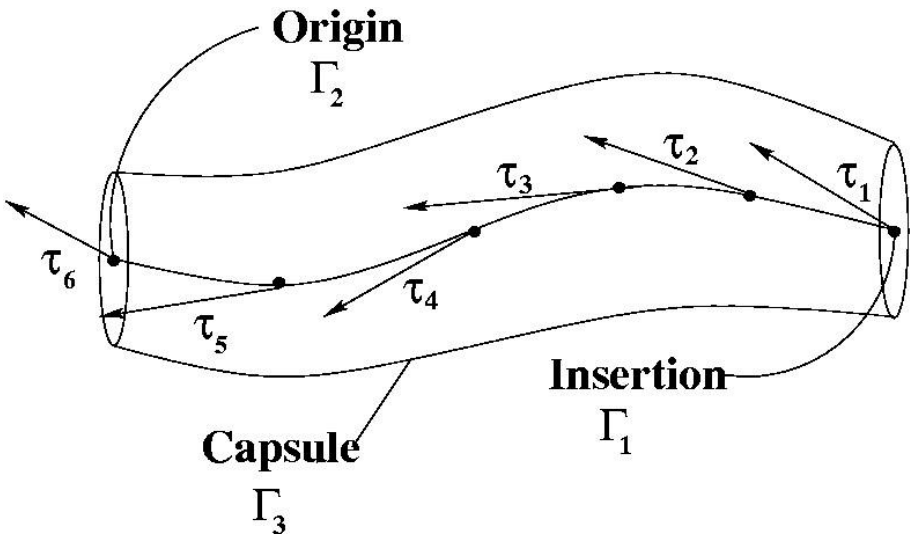

Figure 7.5: Fiber tangents can be interpolated as a kind of flow-field τ running from the insertion Γ_1 to the origin area Γ_2 of muscle.

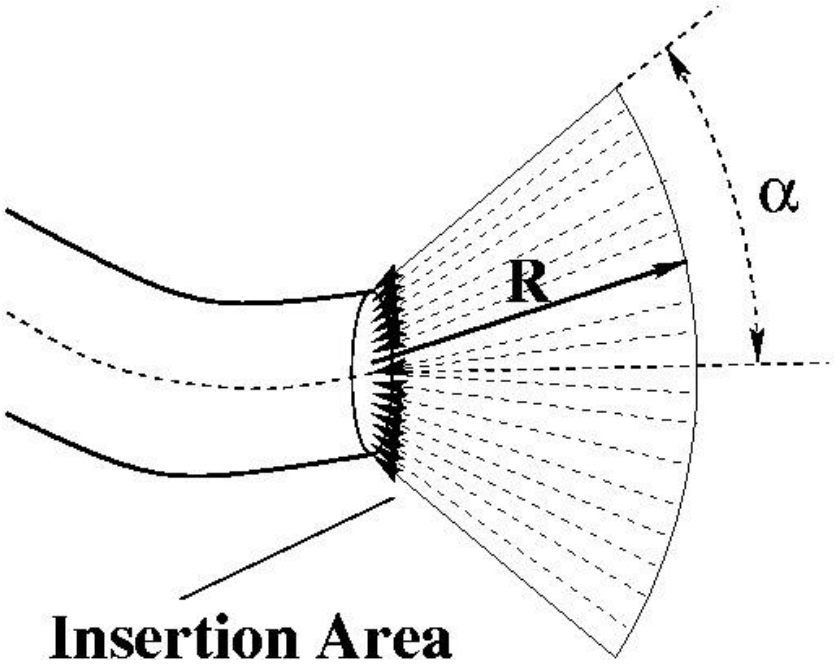

Figure 7.6: Simplified geometrical model of the insertion area.

Artificial model. To validate the approach for modeling of contracting muscle described above, a simulation with a simple artificial model consisting of two nested cylinders is carried out, see Figure 7.7. In this artificial model, the inner cylinder represents muscle and the outer cylinder corresponds to the remaining soft tissue. The areas Γ_i in the BVP (7.7) required for the interpolation of fiber tangents $\boldsymbol{\tau}$ have been assigned as follows: Γ_1 - the top, Γ_2 - the bottom and Γ_3 - the hull of the inner cylinder. The simulation shown in Figure 7.7 is performed within two following steps:

1. First, the vector field of fiber tangents $\boldsymbol{\tau}$ for the inner cylinder is calculated by solving the BVP (7.7).

2. Then, the deformation of the surrounding material under the impact of the force density $\mathbf{f}$ acting along the lines of action $\boldsymbol{\tau}$ precalculated in step (1) is computed by solving the BVP (3.50) with the inhomogeneous right side. Thereby, the deformation of both cylinders in step (2) is computed with the homogeneous essential boundary conditions on the bottom of the outer cylinder $\Gamma_{\text{essential}}$, and natural boundary conditions on the remaining boundary Γ_{natural}.

Since the interpolated orientation of fibers in this example is trivial, namely along the main axis of the inner cylinder, the result of this simulation is as expected.

Facial expressions: feasibility study. In the first feasibility study, the basic postoperative facial expressions for the patient with congenital mandibular hypoplasia (see Section 6.2) is estimated. The result of the static soft tissue prediction for this patient shown in Figure 6.12 was used as an input for further simulation of muscle-based facial expressions. Figure 7.8 (a) shows the transparent geometric model of the patient's head with two mimic muscles, zygomaticus major left and right, which have been identified and segmented from CT data. These particular mimic muscles raise the angle of mouth and are essential for normal smile. Similar to the example with an artificial model, the surface of each muscle is subdivided into three areas $\Gamma_{1,2,3}$, cf. Figure 7.4: the area Γ_1 corresponds to the contact surface between muscle and bone (the origin), Γ_2 is the contact surface to soft tissue in the area of angle of the mouth (the insertion) and Γ_3 is assigned to the remaining muscle capsule. The simulation is performed as following:

1. First, the vector field of fiber tangents $\boldsymbol{\tau}$ for each muscle $\mathcal{M}$ is calculated by solving the BVP (7.7) in $\Omega_{\mathcal{M}}$ with $\Gamma_i \subset \Omega_{\mathcal{M}}$ assigned as mentioned above.

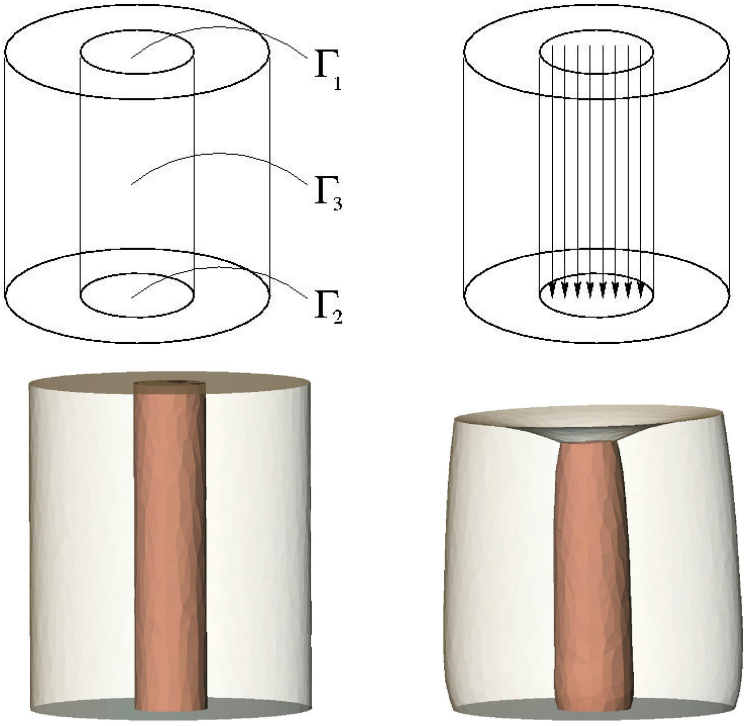

Figure 7.7: From top to bottom, from left to right: allocation of areas Γ_i for the BVP (7.7), estimated orientation of virtual fibers, the original model, simulation of contraction of the inner cylinder and resulting deformation of the remaining material.

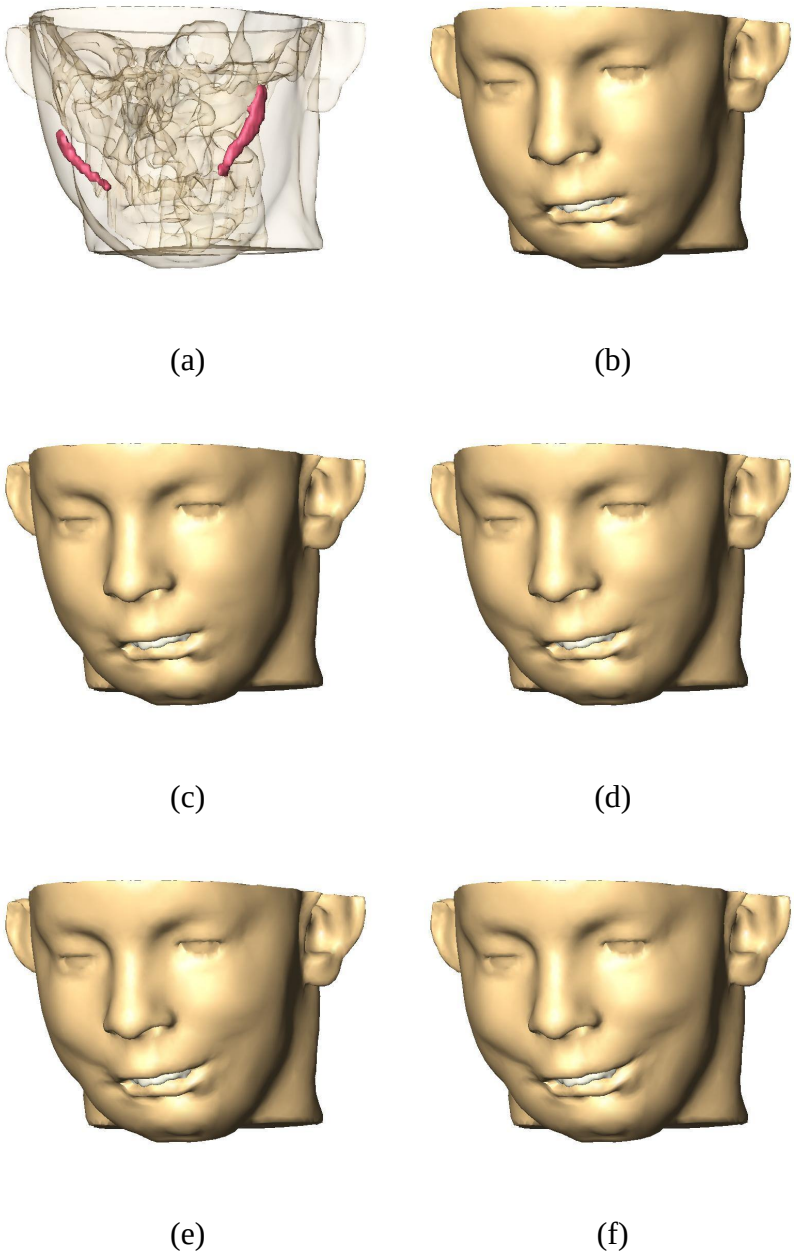

(a) (b)

(c) (d)

(e) (f)

Figure 7.8: Simulation of facial expressions induced by contraction of zygomaticus major left and right. (a): 3D model of patient's head, including muscles, (b): undeformed original surface model, (c-f): resulting soft tissue deformation induced by the increasing contraction of two facial muscles.

2. Then, the force field for the insertion area of each muscle is interpolated. The insertion area of zygomaticus major is parameterized with $R = 0.6$cm and $\alpha = 28$, cf. Figure 7.6.

3. Finally, the deformation of the surrounding facial tissue under the impact of the force density $\mathbf{f} = \lambda \boldsymbol{\tau}$ acting along fiber tangents precalculated in step (1-2) is computed for the range of magnitudes $\lambda_i : \lambda_0 = 0 < \lambda_1 < \lambda_2 ... < \lambda_n = \lambda_{\text{max}}$ by solving the BVP (3.50), see Figure 7.8.

Parameter estimation. Physically based simulation of facial expressions requires numerous parameters to get smart control on the muscle-based soft tissue deformation. Some of them can be computed semi-automatically, while the others can be estimated only empirically. Table 7.1 gives an overview of parameter estimation approaches applied in this work for the simulation of facial expressions.

Table 7.1: Parameter estimation for the simulation of facial expressions.

Parameter	Estimation approach
individual anatomy	tomographic data segmentation
lines of muscle action	shape-based interpolation
geometry of insertion area	empirically
magnitude of muscle forces	empirically
relative stiffness of tissue layers	empirically

An additional problem arises by the modeling of facial tissue deformation under the impact of muscle forces. The intermediate results of the first feasibility study have shown that the aspired realism of the simulation results cannot be achieved on the basis of a homogeneous, "one material"-approximation of facial tissue, which has been applied for the static soft tissue prediction. In particular, the relative stiffness of muscle- and skin-layer is of crucial importance for the modeling of realistic skin deformations. By varying the quotient E_M/E_S, some undesirable effects on the deformed facial surface can be avoided.

FACS-based animation. Facial emotion expressions are the result of interaction between contracting mimic musculature and the surrounding facial tissue. The most rigorous approach to the realistic modeling of complex facial emotion expressions is to utilize natural coding schemes such as the Facial Action Coding System (FACS) developed by Ekman and Friesen [35] in order to calibrate actions

of different groups of facial muscles. The muscle-based abstraction provided by FACS maps well into a facial animation control strategy and has been used in a number of facial animation systems [93, 72]. In Table 7.2, examples of FACS-coded facial emotion expressions are shown.

The coding of complex facial emotion expressions in accordance with FACS is formally equivalent to a superposition of single muscle actions yielding the total displacement field $\mathbf{u}$, i.e.,

$$\mathbf{u} = \sum_i w_i \mathbf{u}^i \tag{7.8}$$

where $w_i \in [0, 1]$ is the weighting factor of the displacement field $\mathbf{u}^i$ corresponding to i-th muscle action. However, (7.8) can strictly be used only for the linear elastic approximation of the soft tissue deformation. In the case of the non-linear approximation, the deformation of soft tissue induced by the simultaneous contraction of N muscles cannot be reduced to the linear combination (7.8) and has to be computed for every unique superposition of muscle actions anew by putting the total sum of all muscle forces $\sum_i^N \mathbf{f}^i$ into the right-hand side of the BVP (3.50).

Advanced simulations of facial expressions. The results of the first experimental study carried out with a relatively simple geometrical model have shown that the simulation of complex facial emotion expressions on the basis of correct geometrical models of human anatomy and consistent biomechanical approaches is feasible. To improve the realism of the simulation results, we further focus on the following aspects:

1. Generalization of the modeling approach for the simulation of complex facial emotion expressions requires more detailed geometrical models, including all groups of mimic muscles.

2. Preliminary experimental results have shown that the parameters determining the insertion area of linear muscles, i.e., its geometry and the acting forces, are decisive for the achievement of realistic results. Accordingly, the estimation of these parameters for each mimic muscle is important for the advanced simulations. Also, the modeling of sphincter muscles such as orbicularis oris requires another parameterization as in the case of linear muscles.

3. The realism of the first simulations was limited by the lack of subtle details, especially around the mouth. For instance, the contact between relatively thin lips and teeth makes a non-trivial problem for the FEM-based modeling.

Table 7.2: FACS: Single Action Units (AU), cf. Figure 7.9.

AU No.	FACS Name	Muscular Basis
1	Inner Brow Raiser	Frontalis, Pars Medialis
2	Outer Brow Raiser	Frontalis, Pars Lateralis
4	Brow Lowerer	Depressor Glabellae, Depressor Supercilli, Corrugator
5	Upper Lid Raiser	Levator Palebrae Superioris
6	Cheek Raiser	Orbicularis Oculi, Pars Orbitalis
7	Lid Tightener	Orbicularis Oculi, Pars Palebralis
8	Lips Toward Each Other	Orbicularis Oris
9	Nose Wrinkler	Levator Labii Superioris, Alaeque Nasi
10	Upper Lip Raiser	Levator Labii Superioris, Caput Infraorbitalis
11	Nasolabial Furrow Deepener	Zygomaticus Minor
12	Lip Corner Puller	Zygomaticus Major
13	Cheek puffer	Caninus
14	Dimpler	Buccinnator
15	Lip Corner Depressor	Triangularis
16	Lower Lip Depressor	Depressor Labii
17	Chin Raiser	Mentalis
18	Lip Puckerer	Incisivii Labii Superioris and Inferioris
20	Lip Stretcher	Risorius
22	Lip Funneler	Orbicularis Oris
23	Lip Tightner	Orbicularis Oris
24	Lip Pressor	Orbicularis Oris
25	Lips Part	Depressor Labii or Relaxation of Mentalis or Orbicularis Oris
26	Jaw Drop	Masetter, Temporal and Internal Pterygoid
27	Mouth Stretch	Ptergoids, Digastric
28	Lip suck	Orbicularis Oris
38	Nostril Dilator	Nasalis, Pars Alaris
39	Nostril Compressor	Nasalis, Pars Transversa, Depressor Septi Nasi
41	Lid Droop	Relaxation of Levator Palpebrae Superioris
42	Slit	Orbicularis Oculi
43	Eyes Closed	Relaxation of Levator Palpebrae Superioris
44	Squint	Orbicularis Oculi, Pars Palpebralis
45	Blink	Relaxation of Levator Palpebrae and Contraction of Orbicularis oculi, Pars Palpebralis
46	Wink	Orbicularis Oculi

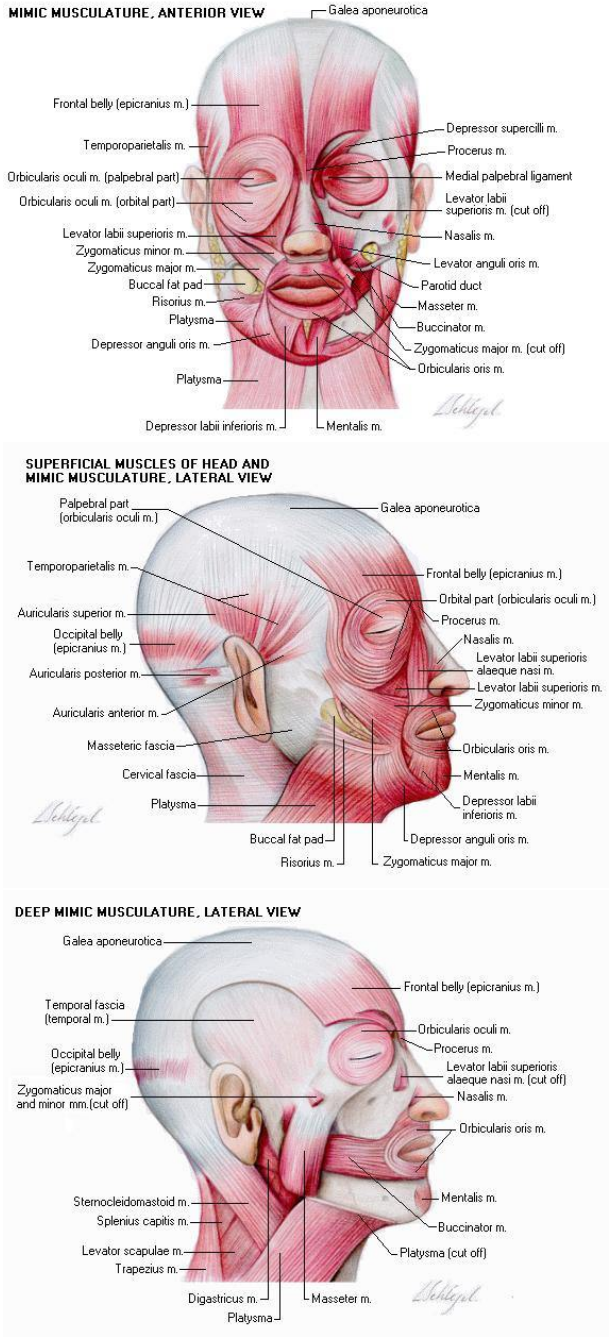

Figure 7.9: Top: mimic musculature, anterior view; middle: superfi cial muscles of head and mimic muscles, lateral view. Bottom: deep mimic musculature, lateral view (from [25]).

Detailed geometrical model of facial musculature. For the advanced simulation of facial emotion expressions, a detailed model of human head, including all groups of mimic muscles, is generated. For this purpose, MRI volunteer data were used, see Figure 7.11.

Parameterization of linear muscles. The parameterization of linear muscles basically consists in the interpolation of fiber tangents for a given muscle shape and the estimation of the insertion area parameters. Since the impact of a muscle on soft tissue is mainly concentrated in the insertion area, i.e., the magnitude of the effective forces acting within the insertion area is much larger than that of the forces inside the muscle, the vector field of fiber tangents (inside of muscle!)τ is not critical for the modeling of single muscle actions and can be intrepolated with any suitable heuristic approach. Instead of the relatively circumstantial, physically motivated interpolation technique used in the first experimental study, we now apply a B-spline based approach to estimate initial lines of muscle forces [118]. The geometrical parameters of the insertion area are estimated empirically. Table 7.3 gives an overview of the insertion area parameters for some linear mimic muscles.

Table 7.3: Parameterization of the insertion area of some linear mimic muscles by the effective radius R of action and the apex angle α, cf. Figure 7.6.

Muscle	R, cm	α
zygomaticus major	0.8	30
zygomaticus minor	0.5	30
risorius	0.5	25
depressor angularis oris	0.7	28
levator angularis oris	0.7	30
depressor labii	0.4	30
levator labii	0.4	30

Parameterization of sphincter muscles. Forces produced by the contraction of sphincter muscles are, in general, difficult to model on the basis of underlying "sliding fibers" mechanism. For example, the impact of orbicularis oris on soft tissue, i.e., the resulting mouth articulation, also depends on the reaction from the teeth. Continuum-based modeling of these phenomena is non-trivial. Instead of this approach, we apply a parameterization technique well known from computer animation, which consists in a heuristic interpolation of sphincter muscles as an ellipsoid contracting along its radial directions, see Figure 7.10.

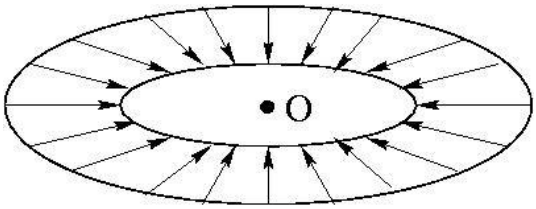

Figure 7.10: Simplified model of sphincter muscle.

Mouth area modeling. The contraction of most mimic muscles results in the deformation of the mouth area. The movements of the lips as well as the resulting form of the mouth are essential elements of the facial emotion expressions. Thus, any incorrectness in the modeling of the mouth area immediately results in unrealistic constraints between the lips and the teeth. In order to enable the natural lips movements, we now treat the contact between lips and teeth as "unfixed", i.e., the natural (Neumann-like) or sliding boundary condition.

Simulation results. Since any facial emotion expression can be obtained as a combination of single muscle actions and basic mouth articulations (e.g., mandible left, right, up, down, forwards and backwards movements), we firstly compute all elementary sequences needed for the modeling of more complex facial emotion expressions. Figure 7.12 illustrates the results of the simulation the basic articulation. The boundary conditions for these simulations are given by the prescribed displacements of mandible. In Figures 7.13-7.16, the simulation results of single muscle actions are shown. In the case of facial muscles, boundary conditions are given by the forces, which have been precalculated as described above. Based on the entire set of precalculated single muscle actions, the complex facial emotion expressions are simulated. Figure 7.17 demonstrates the simulation of a facial expression of happiness estimated by superpositioning single muscle actions of zygomaticus major, zygomaticus minor, risorius and orbicularis oris. Figure 7.18 illustrates a facial expression of disgust simulated as a superposition of single muscle actions of depressor angularis oris left, depressor labii left, mentalis left, levator labii right and orbicularis oris left and right.

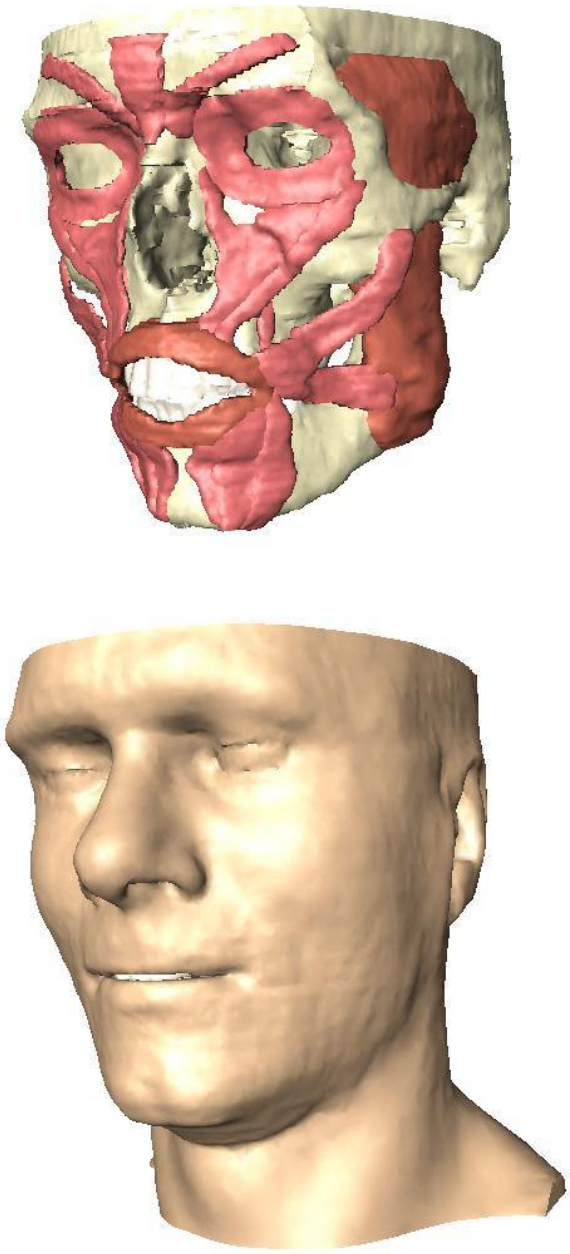

Figure 7.11: Detailed geometrical model of human head generated on the basis of MRI volunteer data (from [118]). Top: inner view, surface model of mimic musculature. Bottom: outer view, skin surface.

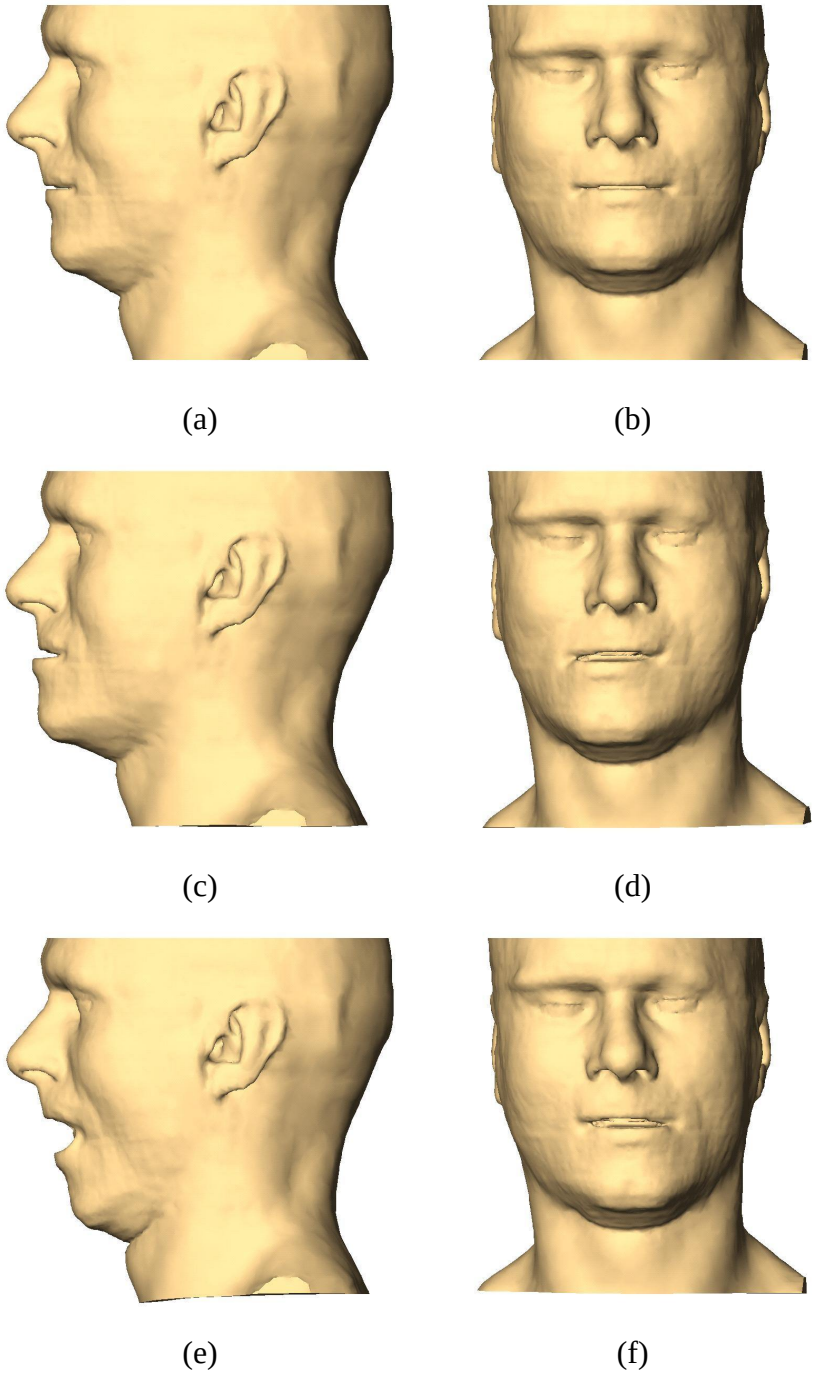

(a) (b)

(c) (d)

(e) (f)

Figure 7.12: Simulation of mandible articulation. (a): original model, lateral view. (b): original model, front view. Mandible movements: (c): forward, (d): right, (e): down, (f): left.

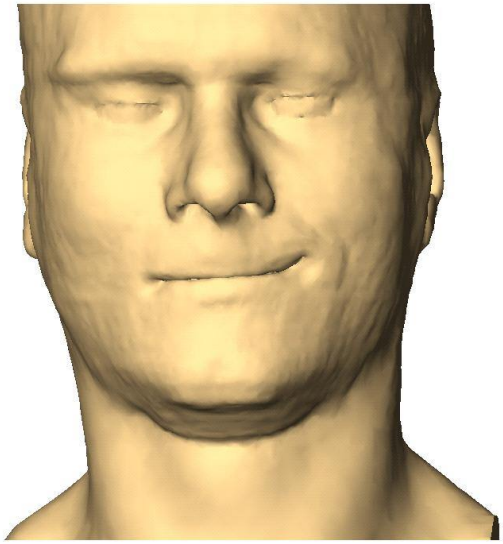

Figure 7.13: Simulation of single muscle action: zygomaticus major left.

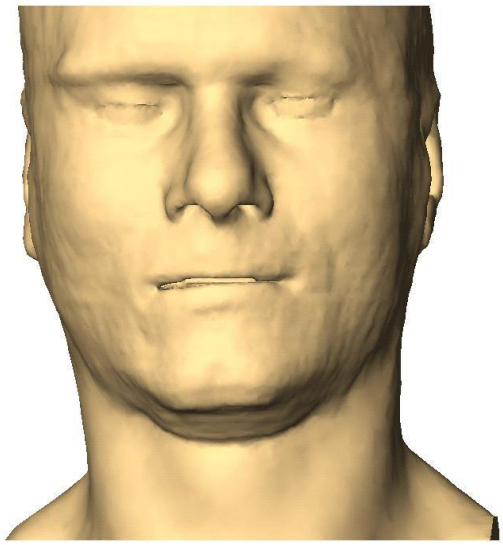

Figure 7.14: Simulation of single muscle action: depressor angularis oris right.

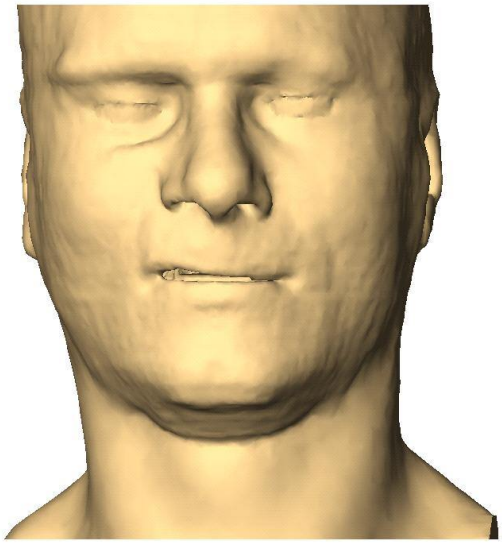

Figure 7.15: Simulation of single muscle action: levator labii right.

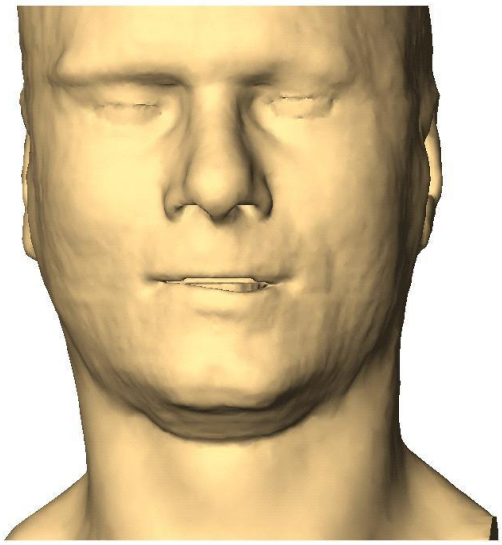

Figure 7.16: Simulation of single muscle action: mentalis left.

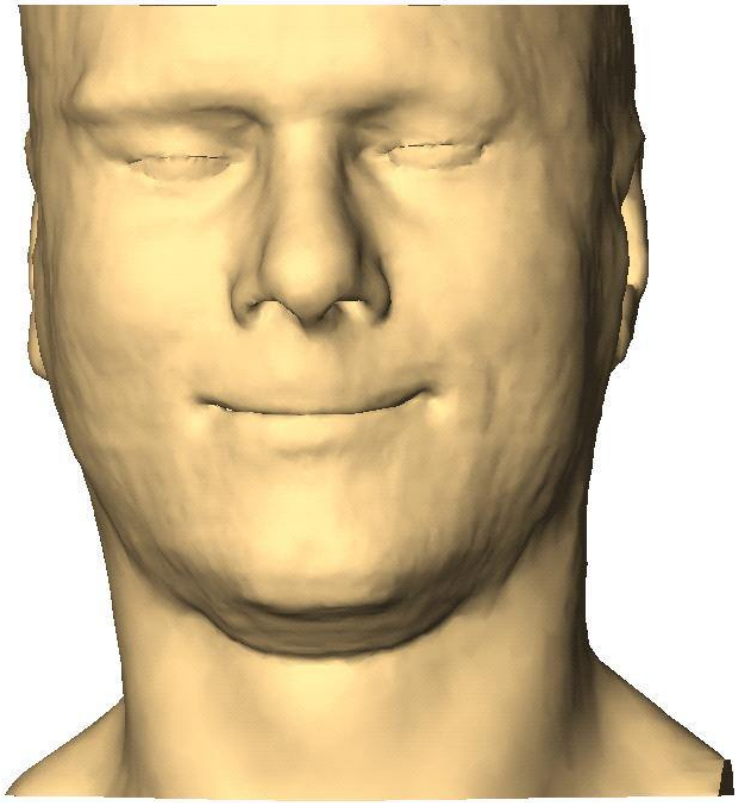

Figure 7.17: Simulation of facial expression of happiness by superpositioning single muscle actions of zygomaticus major, zygomaticus minor, risorius and orbicularis oris.

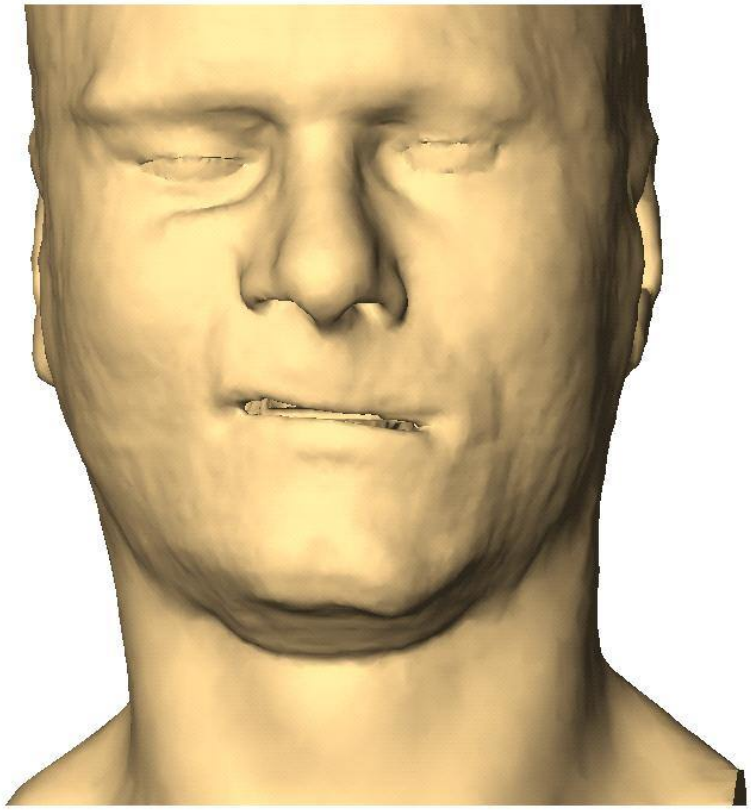

Figure 7.18: Simulation of facial expression of disgust by superpositioning single muscle actions of depressor angularis oris left, depressor labii left, mentalis left, levator labii right and orbicularis oris left and right.